Sensor placement with optimal damage detectability for statistical damage detection

Alexander Mendler, Michael Döhler, Carlos E Ventura

Sensor placement with optimal damage detectability for statistical damage detection

Alexander Mendler[a,b,*], Michael Döhler[b], Carlos E. Ventura[a]

[a] *University of British Columbia, CEME, 6250 Applied Science Lane, Vancouver BC, V6T 1Z4, Canada*
[b] *Université Gustave Eiffel, Inria, COSYS-SII, I4S, Campus de Beaulieu, 35042 Rennes, France*

Abstract

Damage diagnosis based on global structural vibrations critically depends on the sensor layout, in particular when a small number of sensors is used for large structures under unknown excitation. This paper proposes a sensor placement strategy that yields an optimized sensor layout with maximum damage detectability in selected structural components. The optimization criterion is based on the Fisher information, which quantifies the information that the damage-sensitive feature carries on the design parameters of structural components, such as material constants or cross-sectional values. It is evaluated using a finite element model, and considers the statistical uncertainties of the damage-sensitive feature. The methodology is shown for the stochastic subspace-based damage detection method, but can be applied to any damage-sensitive feature whose distribution can be approximated as Gaussian. It is suitable to find the optimal layout for a fixed number of sensors and to choose an appropriate number of sensors. Since the Fisher information is defined component-wise, the sensor layout can be tuned to become more sensitive to damage in local structural components, such as damage hotspots, non-inspectable components, or components that are critical for the safety and serviceability of the structure. For proof of concept, the sensor layout on a laboratory beam is optimized based on numerical simulations, and it is showcased that the optimal sensor layout leads to the highest damage detectability for experimental data.

Keywords: Optimal sensor placement, structural health monitoring, ambient vibrations, Gaussian feature, statistical damage detection, Fisher information

1. Introduction

Modern societies are heavily dependent upon structural and mechanical systems, such as bridges, power plants, off-shore platforms, or wind turbines. To guarantee the safety and serviceability of these structures, periodically scheduled on-site inspections are conducted by trained personnel, and structural health monitoring (SHM) systems are installed. This process of SHM involves the observation through permanently installed sensors, the extraction of damage-sensitive features for data reduction, and their subsequent statistical evaluation using smart algorithms [1]. This way, structural damage can be detected online, triggering on-demand inspections after sudden and unexpected damages or extreme events, such as storms, floods, earthquakes, or impacts of any sort. In particular, output-only vibration-based methods based on the global system response

*Corresponding author; *E-mail address: alexander.mendler@ubc.ca*

to unknown excitation have been actively developed, because they can be applied under normal operating conditions and with relatively few vibration sensors. It goes without saying that the success of such methods heavily depends on a strategic sensor placement.

In recent literature reviews [2–4], numerous *optimization criteria* can be found to optimize the sensor placement for output-only methods. Low-level performance criteria aim to precondition the signal and optimize the signal-to-noise ratio. The measured signal contains information on natural frequencies, damping ratios, and mode shapes. To reduce the noise components, the mode shape observability and amplitude are used as performance criteria, including metrics such as the mode shape summation plot [5], the average driving point residue [6], the eigenvalue vector product [7], or the kinetic energy per mode [8]. The redundancy of information is also considered as a low-level criterion and could be quantified through the mutual information criterion [9]. More advanced criteria aim to optimize the quality of the modal system identification. On one hand, this second group of criteria aims to maximize the identifiability and distinguishability of modes quantified through the modal assurance criterion [10], the modal clarity criterion [11], and the singular value decomposition ratio (i.e. the condition number) [2]. On the other hand, this group of methods attempts to reduce the uncertainty in the estimation through measures such as the information entropy [12–14], the covariance of the state prediction error during Kalman filtering [15, 16], and the Fisher information on the modal contribution of sensor locations [8]. In the latter case, optimization criteria are formed based on the matrix determinant [8], the minimum singular value [17], the singular value decomposition ratio [18], or the absolute values of the main diagonal terms. Criteria such as the kriging prediction error [19] and the representative least-square [20] moreover allow for the minimization of uncertainties at unmeasured degrees of freedom. Recent literature reviews emphasize that there is a need to develop method-specific performance criteria that are tailored to the employed damage diagnosis method [2, 4]. Such high-level criteria that target the detectability of damage directly are rare [21, 22], and typically require supervised training using numerical data from numerous damage states [23]. Moreover, none of the existing criteria appear to consider the detectability of changes in selected structural components, which is the focus of this paper. Considering that optimal damage detectability in all components with a limited number of sensors is unrealistic, the goal is to develop an optimization criterion that targets a prioritized set of damage scenarios. Such damage hotspots are typically known from the operational evaluation of the structure and should be considered during sensor placement.

Finding the optimal sensor layout is not straightforward, regardless of the chosen optimization criterion discussed above. In most cases, the number of possible sensor combinations is excessively large, and it is infeasible to evaluate all combinations in an exhaustive search (ES). To remedy this, smart *optimization methods* are applied. Most performance criteria for sensor placement are non-differentiable, meaning the relation between input and output cannot be described through analytical functions, and deterministic optimization methods (which evaluate the gradient or Hessian matrix) are rarely used [2]. Sequential sensor placement (SSP) methods, where the optimal sensor configuration is found by systematically adding or removing a subset of channels in each iteration step [24], are efficient, at least for single-objective optimization [12]. However, the solution depends on the initial sensor choice and the number of sensors that are removed at the time, and there is no guarantee that the optimal solution can be found [25]. Stochastic optimization methods are more appropriate, as they combine local search with coordinated global search techniques, and randomized local and global elements to overcome local minima. One of the most prominent groups are genetic algorithms (GAs) [26]. Other methods include simulated annealing [27, 28], particle swarm

optimization [29], the distributed wolf method [30], the ant colony optimization method [31], the artificial bee colony method [32], the firefly algorithm [33], the micro-habitat frog leaping method [34], and the monkey algorithm [35], with an overview in [3, 4].

The objective of this paper is to develop a sensor placement strategy that optimizes the detectability of damage in selected structural components, and to combine it with a genetic algorithm to efficiently find a close-to-optimal sensor layout for large structures. A performance criterion is derived for statistical damage detection tests and damage-sensitive features that are (approximately) Gaussian distributed, such as the stochastic subspace-based residual [36–39]. The statistical test considers the uncertainties in the feature and the sensitivity toward changes in structural components, calculated based on a finite element (FE) model. Using the Fisher information [39, 40], the information from the sensitivity analysis and the uncertainty estimation are combined and a performance criterion is developed, which takes as input the desired detectable damage in percent of local structural design parameters. Particular features of the approach are that the sensor layout can be optimized based on the undamaged structure and that it can be tuned to maximize the damage detectability in selected structural components, e.g. damage hotspots, or other components that are critical for the safety and serviceability of the structure. The resulting sensor placement strategy is suitable to find an optimal sensor layout, and can help to choose an appropriate number of sensors. Keeping in mind that no data is available from real structures before sensors are installed, the developed sensor placement strategy is validated based on numerical simulations and verified with experimental data of a laboratory beam. The results showcase that the optimal sensor layout leads to the highest damage detectability.

The paper is organized as follows: Section 2 gives background on the statistical damage detection methods for which the sensor layout will be optimized. Section 3 proposes the sensor placement strategy. In Section 4, the approach is applied to a pin-supported beam, where the sensor layout is optimized based on simulated data, with an experimental proof of concept study in Section 5. Ultimately, the paper is concluded in Section 6.

2. Statistical Damage Detection

2.1. Damage-sensitive Residual

Suppose that a consistent estimate of a damage-sensitive feature vector $\hat{\mathbf{x}} = [\hat{x}_1, \ \dots \ , \ \hat{x}_G]^T$ is available from the measurements of a monitored system, computed from a measurement record of sample size N. Further suppose that damage manifests itself in a deviation of the feature mean; then, a damage-sensitive *residual vector* $\boldsymbol{\varepsilon}$ can be defined by normalizing the feature by its mean vector $\boldsymbol{m} = \mathrm{E}(\hat{\mathbf{x}})$ in the reference state, with

$$\boldsymbol{\varepsilon} = \hat{\mathbf{x}} - \boldsymbol{m}. \tag{1}$$

If the underlying measurements are assumed to be the realizations of a stationary stochastic process, the vector $\boldsymbol{\zeta} = \sqrt{N}\boldsymbol{\varepsilon}$ is often asymptotically normal distributed [41]

$$\boldsymbol{\zeta} = \sqrt{N}\boldsymbol{\varepsilon} \longrightarrow \mathcal{N}(\mathbf{0}, \boldsymbol{\Sigma}) \quad \text{(reference state)} \tag{2}$$

where the mean vector is zero, and $\boldsymbol{\Sigma}$ is the covariance of the Gaussian residual vector $\boldsymbol{\zeta}$, describing the dispersion about the mean due to stochastic loads and measurement noise. In other words, the distribution of the residual can be approximated by a normal distribution when computed on sufficiently large sample size N—a criterion that is met by many features from the literature, e.g.

modal parameters [42, 43] or features that are formed based on the subspace properties of output covariance Hankel matrices [36, 37, 44, 45]. Some features from the literature [46–48] are even robust to changes in environmental conditions. In Appendix A, an exemplary Gaussian residual vector is given, i.e. the stochastic subspace-based residual, which will be used to demonstrate the developments in this paper.

2.2. Damage Parametrization and Detection

For meaningful damage detection, the data-driven features from the previous section have to be linked to monitoring parameters $\boldsymbol{\theta}$ that characterize the structural system, e.g. design parameters of local structural components. This way, structural damage can be defined as a deviation of the monitoring vector from its reference vector, $\boldsymbol{\theta} - \boldsymbol{\theta}^0$, and the effect on the damage-sensitive feature can be described through the first-order Taylor expansion

$$\mathrm{E}_{\boldsymbol{\theta}}[\boldsymbol{\varepsilon}] \approx \mathrm{E}_{\boldsymbol{\theta}^0}[\boldsymbol{\varepsilon}] + \boldsymbol{\mathcal{J}}(\boldsymbol{\theta} - \boldsymbol{\theta}^0), \tag{3}$$

where $\boldsymbol{\mathcal{J}} = \frac{\partial \mathrm{E}_{\boldsymbol{\theta}}[\boldsymbol{\varepsilon}]}{\partial \boldsymbol{\theta}}\Big|_{\boldsymbol{\theta}=\boldsymbol{\theta}^0}$ is the first-order sensitivity matrix (the Jacobian matrix), and $E_{\boldsymbol{\theta}}$ is the expected value of a random variable calculated under system parameter $\boldsymbol{\theta}$. Due to the formulation as a residual vector, the expected value in the reference state is zero, i.e. $\mathrm{E}_{\boldsymbol{\theta}^0}[\boldsymbol{\varepsilon}] = 0$. To characterize the residual vector in the damaged state, the following damage hypotheses about the system states are made [49]

$$\begin{array}{ll} H_0: \ \boldsymbol{\theta} = \boldsymbol{\theta}^0 & \text{(reference state)} \\ H_1: \ \boldsymbol{\theta} = \boldsymbol{\theta}^0 + \boldsymbol{\delta}/\sqrt{N} & \text{(damaged state)}, \end{array} \tag{4}$$

where

$$\boldsymbol{\delta} = \sqrt{N}(\boldsymbol{\theta} - \boldsymbol{\theta}^0) \tag{5}$$

is the asymptotic change vector. Then, the distribution of the Gaussian residual vector in the reference and the damaged state for $N \to \infty$ results in [49]

$$\boldsymbol{\zeta} = \sqrt{N}\boldsymbol{\varepsilon} \longrightarrow \begin{cases} \mathcal{N}(\mathbf{0}, \boldsymbol{\Sigma}) & \text{(reference state)} \\ \mathcal{N}(\boldsymbol{\mathcal{J}}\boldsymbol{\delta}, \boldsymbol{\Sigma}) & \text{(damaged state)}, \end{cases} \tag{6}$$

meaning damage manifests itself in a deviation in the mean of the Gaussian residual vector. Based on these properties, statistical hypothesis tests can be applied to decide if the residual corresponds to the reference or to the damaged state. The corresponding test statistic [38]

$$t = \boldsymbol{\zeta}^T \boldsymbol{\Sigma}^{-1} \boldsymbol{\mathcal{J}} \left(\boldsymbol{\mathcal{J}}^T \boldsymbol{\Sigma}^{-1} \boldsymbol{\mathcal{J}} \right)^{-1} \boldsymbol{\mathcal{J}}^T \boldsymbol{\Sigma}^{-1} \boldsymbol{\zeta} \sim \begin{cases} \chi^2(\nu, 0) & \text{(reference state)} \\ \chi^2(\nu, \lambda) & \text{(damaged state)} \end{cases} \tag{7}$$

is approximately χ^2-distributed, where the distribution is characterized through the number of degrees of freedom

$$\nu = \mathrm{rank}(\boldsymbol{\mathcal{J}}^T \boldsymbol{\Sigma}^{-1} \boldsymbol{\mathcal{J}}) \tag{8}$$

and the non-centrality

$$\lambda = \boldsymbol{\delta}^T \left(\boldsymbol{\mathcal{J}}^T \boldsymbol{\Sigma}^{-1} \boldsymbol{\mathcal{J}} \right) \boldsymbol{\delta}. \tag{9}$$

The non-centrality from Eq. (9) describes the mean test response, i.e. the shift in the mean value of the test distribution due to the change $\boldsymbol{\delta}$, see Fig. 1. The test statistic from Eq. (7) is a scalar value, and an alarm is issued if the test statistic exceeds a safety threshold value $t > t_{crit}$. This threshold is typically calculated in the training state based on the acceptable probability of false alarms (PFA) [39].

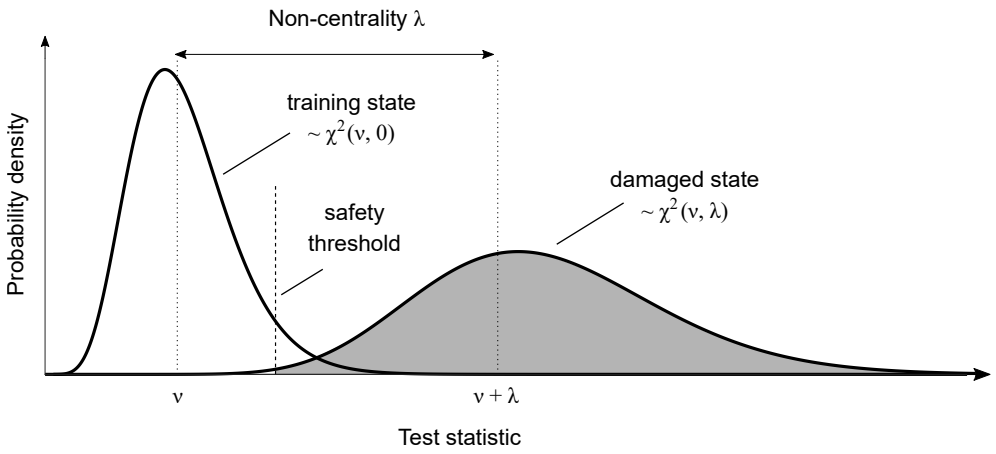

Figure 1: Reliability considerations based on the χ^2-distribution of the test statistic.

3. Sensor Placement Strategy

The primary goal of the sensor placement is to optimize the detectability of local damages. To achieve this goal, it has to be defined what damage is, and its effect on the statistical detection test has to be quantified. A common approach is to discretize the structure, i.e. to divide it into finite elements (FEs) and to form structural components by assigning the same structural design parameter θ_h to all FEs within one component. Then, the physical system can be characterized through a parameter vector $\boldsymbol{\theta} = [\theta_1, \ \dots \ , \ \theta_H]^T \in \mathbb{R}^H$, which typically contains material constants or cross-sectional values, and damage can be parametrized as a deviation in the parameter vector from the reference values $\boldsymbol{\theta}^0$ through the vector $\boldsymbol{\theta} - \boldsymbol{\theta}^0$.

The effect of damage on the damage-sensitive residual vector can be captured with a sensitivity matrix, where each column describes the sensitivity (the first-order derivative) of the damage-sensitive residual vector to one design parameter θ_h with

$$\boldsymbol{\mathcal{J}} = \left.\frac{\partial E_{\boldsymbol{\theta}}[\boldsymbol{\varepsilon}]}{\partial \boldsymbol{\theta}}\right|_{\boldsymbol{\theta}=\boldsymbol{\theta}^0} = \left.\begin{bmatrix} \frac{\partial}{\partial\theta_1}E_{\boldsymbol{\theta}}[\varepsilon_1] & \frac{\partial}{\partial\theta_2}E_{\boldsymbol{\theta}}[\varepsilon_1] & & \frac{\partial}{\partial\theta_H}E_{\boldsymbol{\theta}}[\varepsilon_1] \\ \vdots & \vdots & \dots & \vdots \\ \frac{\partial}{\partial\theta_1}E_{\boldsymbol{\theta}}[\varepsilon_G] & \frac{\partial}{\partial\theta_2}E_{\boldsymbol{\theta}}[\varepsilon_G] & & \frac{\partial}{\partial\theta_H}E_{\boldsymbol{\theta}}[\varepsilon_G] \end{bmatrix}\right|_{\boldsymbol{\theta}=\boldsymbol{\theta}^0} . \tag{10}$$

In case of the subspace-based residual from Appendix A, the residual is first derived with respect to the modal parameters, and secondly, modal parameters are derived with respect to structural parameters $\boldsymbol{\theta}$ in a FE model, so the derivatives can be combined using the chain rule [50]. Whether or not damage is detectable not only depends on the sensitivity $\boldsymbol{\mathcal{J}}$, but also the covariance matrix $\boldsymbol{\Sigma}$, i.e. the uncertainty related to the estimation of the damage-sensitive residual. The Fisher information matrix

$$\mathbf{F} = \boldsymbol{\mathcal{J}}^T\boldsymbol{\Sigma}^{-1}\boldsymbol{\mathcal{J}} = \begin{bmatrix} F_{11} & F_{21} & \dots & F_{H1} \\ & F_{22} & \dots & F_{H2} \\ & & \ddots & \vdots \\ (\text{sym.}) & & & F_{HH} \end{bmatrix} \tag{11}$$

considers both quantities, and is a scaling factor for the mean test response from Eq. (9). The main diagonal values F_{hh} quantify the information content of the residual on each individual design

parameter, and thus, quantify the detectability of changes therein [39]. The off-diagonal values, on the other hand, describe how similar the effect of changes in different parameters is on the residual. Since the Fisher information changes with changing sensor layout, it can be used as a performance criterion for sensor placement optimization [51]. However, to ease the physical interpretation, the next section translates the Fisher information into a more intuitive measure.

3.1. Optimization Criterion

This section explains how the Fisher information can be translated into a meaningful performance criterion for damage detectability. For the following considerations, the effect of changes in a single parameter θ_h is analyzed while assuming no change in the other parameters, simplyfying the mean test response from Eq. (9) to

$$\lambda = \delta_h^2 F_{hh}. \tag{12}$$

Formulating the asymptotic change vector from Eq. (5) for a single parameter change, with $\delta_h = \sqrt{N}(\theta_h - \theta_h^0)$, and substituting it into Eq. (12), while replacing the sample size with the measurement duration and the sampling frequency $N = T f_s$, yields an enhanced formula for the mean test response

$$\lambda = T \cdot (\theta_h - \theta_h^0)^2 f_s F_{hh}. \tag{13}$$

This formula is more intuitive than Eq. (9) because it relates the mean test response to physical quantities, such as the measurement duration during testing T and the absolute parameter change $\theta_h - \theta_h^0$ squared. In particular, it reveals an important property of the statistical damage detection test: the mean test response increases with increased measurement duration when the parameter change is constant. Consequently, smaller damage can be detected with longer measurements.

Eq. (13) gives the user the opportunity to define the requirements toward the diagnosis result as follows: The mean test response λ is a measure for the detectability of damage. On one hand, it should exceed a minimum value $\lambda > \lambda_{min}$, so the distributions are clearly separated, a damaged structure is correctly classified as damaged, and the probability of detection is close to 100%, see Fig. 1. On the other hand, there is no benefit in increasing the mean test response beyond the minimum value, as no further information is gained for damage detection. Hence, a target value $\lambda = \lambda_{min}$ will be set for the optimization. Furthermore, the parameter change $\theta_h - \theta_h^0$ that should be detectable can be defined by the user. When expressed in percent of a reference parameter $\Delta_h = (\theta_h - \theta_h^0)/\theta_h^0$, it becomes an intuitive input parameter to prioritize different structural components during damage detection. With the mean test response and the parameter change in Eq. (13) being fixed through physical considerations, and F_{hh} being determined for a given sensor placement, the required measurement duration follows as

$$T_h = \frac{1}{(\Delta_h \theta_h^0)^2} \frac{\lambda_{min}}{f_s F_{hh}}. \tag{14}$$

The duration T_h is the required measurement duration to detect a specified damage extent Δ_h with the desired test response λ_{min}. An efficient sensor configuration leads to a high Fisher information and a low measurement duration, as less data is necessary to achieve the desired probability of detection. Consequently, it is a comparable measure for damage detectability in the different structural components h, and an appropriate criterion for performance-based sensor placement. More information on how to set the input parameters is given in the following list.

- *Minimum non-centrality λ_{min}:* Fixing the mean test response to a minimum value $\lambda = \lambda_{min}$ is equivalent to requiring a minimum reliability regarding the SHM system. It can be fixed based on an acceptable probability of false alarms (PFA), a code-based reliability index β for assessing existing structures, and the problem-specific number of degrees of freedom $\nu = \text{rank}(\mathbf{F})$ of the χ^2-distribution of the test statistic. The relationship between the minimum non-centrality and the number of degrees of freedom is explained in detail in the referenced literature [39] with the final results being summarized in Fig. 2 for varying reliability indices. Moreover, different reliability levels $\lambda_{min,h}$ can be defined for individual structural components, depending on the damage consequences on local or global level or the accessibility during on-site inspections. Higher reliability could, for example, be required for structural components that are inaccessible, or for components that could cause a total system collapse.

- *Minimum detectable damage Δ_h:* The relative parameter change is a tuning parameter for the damage diagnosis. It enables the user to select relevant design parameters θ_h in the FE model and to define the minimum change in these parameters that has to be sensed by the damage detection method at a pre-defined reliability. This feature is pivotal for global damage detection based on a small number of modes and a sparse sensor layout: irrelevant parameter changes in the global structure can be neglected for the optimization, and the sensor placement can be tuned to become more sensitive to damage hotspots or changes in local components, which are critical for the safety or serviceability of the structure. The framework inherently considers the magnitude of the monitoring parameter and only a relative change is to be specified.

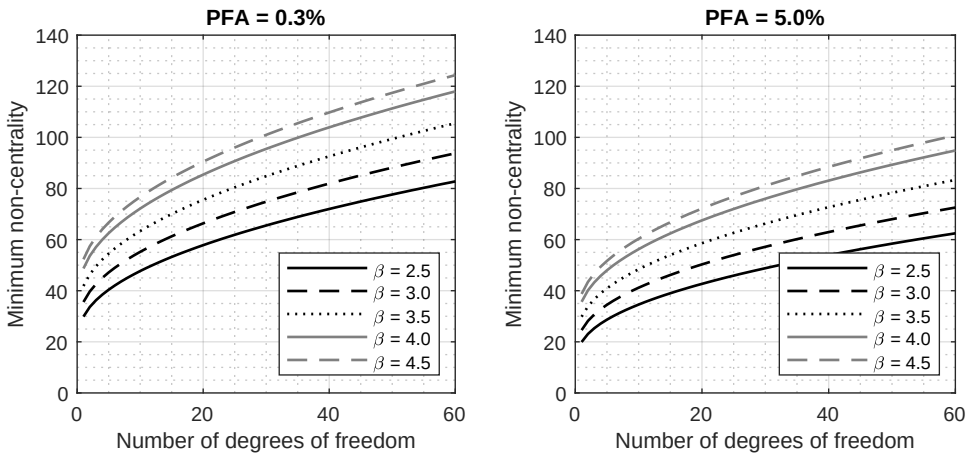

Figure 2: Minimum non-centrality λ_{min} based on the reliability index for assessing structural systems [39].

Among all structural components h, with $h = 1, \ldots, H$, the decisive measurement duration (i.e. the measurement duration for the entire structure) is chosen as the maximum measurement duration

$$T = \max\{T_1, \cdots, T_H\}, \tag{15}$$

as only this duration guarantees the detectability of the specified damages in all considered components. It depends on the sensor configuration c, as well as the number of sensors r. Algorithm 1

summarizes the evaluation of the objective function $T = T(c, r)$. It should be noted that simulated vibration data from the undamaged structure $\mathbf{y} \in \mathbb{R}^{r \times N^0}$ of sample size N^0 is used.

Algorithm 1 Objective function T

Input: FE model with monitoring parameter vector $\boldsymbol{\theta}^0$, sampling frequency f_s, minimum detectable damages Δ_h, PFA, reliability index β

1: If vibration data is not available, generate the measurement matrix $\mathbf{y} \in \mathbb{R}^{r \times N^0}$
2: Estimate the covariance, sensitivity, and Fisher information matrix from Eq. (11) using $\mathbf{y}$;
3: Evaluate the number of degrees of freedom from Eq. (8)
4: Set the minimum non-centrality λ_{min} based on β and the PFA [39]
5: **for** $h = 1$ to H **do**
6: Calculate T_h using Eq. (14)
7: **end for**
8: Calculate T using Eq. (15)

This section showed that a more efficient sensor layout leads to a higher Fisher information F_{hh} (i.e. higher sensitivity and lower uncertainty) and a shorter measurement duration. Consequently, the optimal sensor layout for a fixed number of sensors r can be found as the one with the minimal measurement duration

$$T_{opt}(r) = \min_{c} \{T(c, r)\}. \tag{16}$$

Ultimately, an upper bound for the measurement duration is introduced (i.e. the maximum allowable measurement duration) and the optimization problem is restrained to values below one.

$$\begin{aligned} \min_{c} \quad & f(c, r) \qquad f(c, r) = \frac{T(c, r)}{T_{thres}} \\ \text{s.t.} \quad & f(c, r) \leq 1 \end{aligned} \tag{17}$$

This is an efficient way to remove unsuitable sensor layouts, in which some of the considered damage scenarios are undetectable. Furthermore, it allows one to weigh the objective function if it is to be combined with others in a multi-objective optimization approach. The subsequent sections will show how to find an optimal sensor placement that minimizes T, as well as an appropriate number of sensors.

3.2. Optimization Method

3.2.1. Exhaustive Search

A straightforward way to find the minimum of the optimization function in Eq. (17) is the evaluation of the performance criterion for all possible sensor configurations c in an exhaustive search (ES), and selecting the optimal configuration as the one with the shortest duration. The exhaustive approach is only applicable if the number of possible sensor combinations N_c is reasonably small, because the calculation of the objective function can be computationally expensive. For r sensors and r_{tot} candidate locations, the number of combinations N_c is

$$N_c(r, r_{tot}) = \binom{r_{tot}}{r} = \frac{r_{tot}!}{(r_{tot} - r)!r!}. \tag{18}$$

After simulating a single measurement record with data from all candidate locations, the corresponding channels for each sensor configuration are extracted from the measurement matrix, and the objective function is calculated and stored together with the sensor configuration number c (see Algorithm 1). Ultimately, the optimal sensor configuration number c_{opt} is determined according to Eq. (17) and stored together with the corresponding measurement duration T_{opt}.

3.2.2. Genetic Algorithm

This section describes how to efficiently find a close-to-optimal solution by modifying a genetic algorithm (GA) [52, 53]. GAs are inspired by the natural evolution process based on Darwin's survival of the fittest principle. In this context, the objective function is referred to as the *fitness* function, a single sensor layout is an *individual* that consists of multiple *genes* (i.e. channel numbers), and a *population* is an array of individuals. For sensor placement, the optimization problem is encoded through integer numbers, meaning one gene is an integer channel number and each sensor layout is a vector that includes r numbers. Evolution takes place within a population, i.e. a large set of individuals, where the parent generation contributes its genes to its children through *cross-over, mutation, and elitism* [52]. For the application in this paper, the standard GA is employed that is pre-implemented in the Global Optimization Toolbox in MATLAB but the cross-over and mutation functions are modified. They include a restraint that does not allow for multiple sensors to be placed at the same locations. The mutation rate linearly decreases, meaning initially the number of perturbed channel numbers is high, but with increasing number of iterations (i.e. generations), the intensity of the perturbation gradually reduces.

The optimization is based on a single vibration record at all candidate sensor locations and launches with a random initial population. For each generation, the corresponding channels are extracted from the measurement matrix, the fitness of each individual $i = 1, 2, \ldots, N_i$ is calculated (see Algorithm 1) and scaled using Eq. (17). Based on the elite count, the fittest individuals are passed on to the next generation without modification, and a cross-over fraction determines the number of cross-over and mutation children. The selection of parents for cross-over is made in a tournament selection [54], meaning a user-defined number of individuals (e.g. two individuals) are randomly selected in the current population, and only the fitter one is allowed to reproduce. The algorithm has the population evolve from generation to generation with $g = 1, 2, \ldots, N_g$, and terminates if one of the stopping criteria is met (i.e., a maximum number of generations is exceeded, a maximum computation time has passed, or the optimal solution has not improved by more than a specified tolerance value over a certain period of time or number of generations). Upon termination, the algorithm outputs the ranked elite members of the current population as a set of optimal solutions.

3.3. Appropriate Number of Sensors

The proposed sensor placement strategy is suitable to find an optimal sensor layout as well as an appropriate number of sensors. This is because an increasing number of sensors increases the Fisher information (increased sensitivity or lower uncertainty), and shortens the measurement duration. In any case, the optimization is launched with the minimum possible number of sensors (for example $r = 1$). Then, the number of sensors is gradually increased (from one to two, three, ...) while plotting the optimal measurement duration T_{opt} over the number of sensors r in a *performance curve* and storing the corresponding sensor configuration. One way to decide on an appropriate sensor number is to terminate the optimization once the optimal measurement duration

T_{opt} drops below the maximum allowable measurement duration T_{thres}, with

$$T_{opt} < T_{thres}. \tag{19}$$

Another approach is to plot the optimal measurement duration over a wide range of sensor numbers and to evaluate the elbow point (i.e. the point with the highest curvature of the performance curve) beyond which the measurement duration does not significantly improve. Alternatively, a cost function could be defined that relates the information gain with instrumentation costs. It is important to note that the optimal sensor layout can be entirely different for a different number of channels, meaning it cannot be found through sequential sensor placement, where the optimal sensor configuration is achieved by systematically adding or removing a subset of channels. Ultimately, it should be considered that an increased number of sensors leads to a longer computation time for each iteration and possibly an increased number of sensor combinations.

4. Application to a Steel Beam

In the following, the sensor placement strategy is applied to a pin-supported beam from Fig. 3, where the selected damage-sensitive residual is the stochastic subspace-based residual vector, see Appendix A. All considerations in this section are made based on a numerical model and simulated vibration data, while validation studies based on experimental data are reported in Section 5.

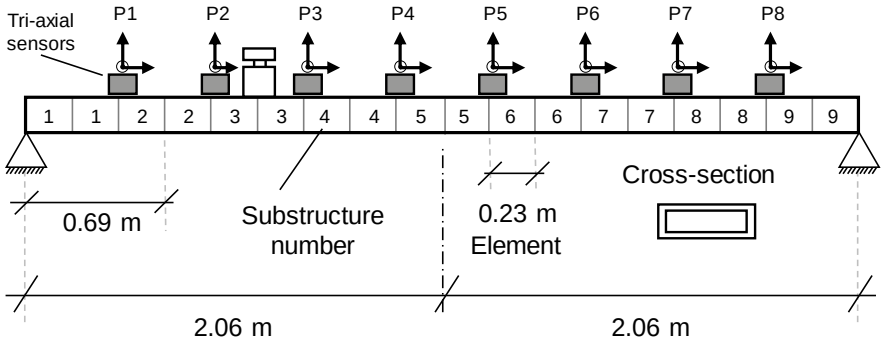

Figure 3: Finite element model of the HSS beam including the possible sensor locations P1-P8

4.1. Structure and Instrumentation

The structure under consideration is a pin-supported beam with a length of 4.11 m, see Fig. 3. It exhibits a total mass of 56.8 kg, a modulus of elasticity of E = 210,000 MPa, and a hollow structural steel cross-section, HSS 152x51x4.78 mm. The supports at both ends are metal bolts in the centreline of the profile, which only allow for a rotation about the weak axis. An input source with a total mass of 3.6 kg is placed 68.5 cm away from the support, injecting white noise vertically into the beam, and eight accelerometers, with a weight of 1.28 kg each, are placed every 0.46 cm. Moreover, a 3-D finite element model with 19 joints and 18 beam elements is created in ANSYS, and possible sensor locations are defined at the positions P1 - P8 from Fig. 3. The shaker and the sensors are modelled as point masses with no rotational mass. Since 18 finite elements are used, the parametrization is limited to the 18 E-Moduli, mass densities, and cross sectional values. In this study, every two consecutive elements are combined to one component by assigning the same

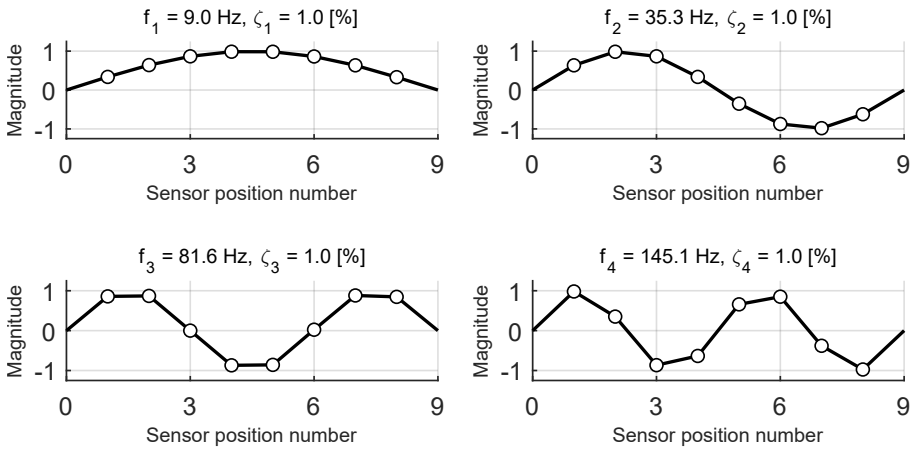

Figure 4: Numerical mode shapes from ANSYS

material properties, see Fig. 3, and damage is defined as a change in structural mass. This leads to nine possible damage locations along the beam, modeled through changes in the respective mass parameters

$$\boldsymbol{\theta} = \begin{bmatrix} m_1 & \dots & m_9 \end{bmatrix}^T \tag{20}$$

with $m_h = 6.31$ kg. For damage diagnosis, the first four modes of vibration in the vertical direction are considered, see Fig. 4. The optimization algorithm requires a vibration record with data from all possible sensor locations, so a single transient analysis is run while storing the accelerations at P1 - P8. For excitation, a Gaussian white noise input signal is applied at a single joint (the shaker location) and in the vertical direction. The output signal is generated using a modal reduction approach and sampled at a frequency of $f_s = 330$ Hz. The measurement duration in the reference state is fixed to 110 min and all other signal processing parameters are summarized in Table B.1.

4.2. Minimum Measurement Duration

In this section, the measurement duration is calculated for a fixed sensor layout, e.g. for a single vertical channel at sensor position P1. According to Eq. (14), the minimum measurement duration depends on the detectable damage, which is set to $\Delta_h = 5\%$ (0.31 kg) for each beam component, and the minimum non-centrality (the minimum mean test response), which is fixed to $\lambda_{min} = 30$. Next, the Fisher information from Eq. (11) is calculated based on vibration data from the undamaged structure and on the FE parameter sensitivities. Ultimately, the main diagonals of the Fisher information are extracted and the minimum measurement duration is calculated for each beam component, using Eq. (14), with the results being visualized in Fig. 5 (left side). The measurement duration in beam segment 1 and 9 are not identical because of the asymmetrical mass distribution (the shaker is placed on beam segment 3/9), which causes the mode shapes and the sensitivity matrix to be asymmetrical. The placement of the shaker also leads to more pronounced vibration amplitudes in one half of the beam and modified covariance properties for the respective beam elements. The decisive measurement duration is the maximum measurement duration ($T = T_5 = 442\ s$), which is used as a criterion for sensor placement. For later considerations, the measurement duration is evaluated for two additional sensor layouts—one with two sensors at positions P1 and P8 (Fig. 5, centre), and another with three sensors at P1, P4, and P8 (Fig. 5,

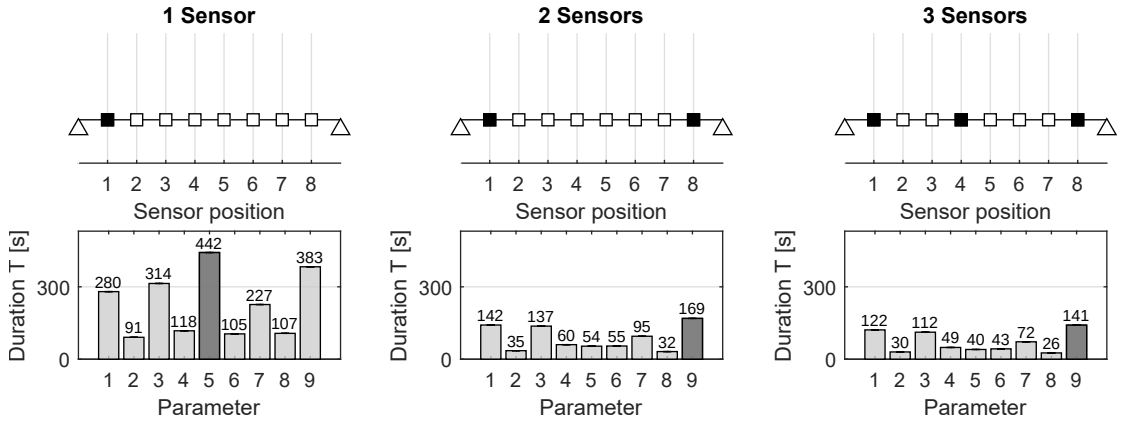

Figure 5: Measurement duration to detect a 5% damage in each mass parameter for a fixed sensor layout

right side). The corresponding maximum measurement durations are $T = 169\ s$ and $T = 141\ s$, respectively.

4.3. Optimal Sensor Layout

a) Exhaustive Search

This section demonstrates how the optimal sensor configuration can be found for a fixed number of sensors, starting with the optimal location for a single sensor, $r = 1$. The approach to evaluate the performance criterion for a fixed sensor layout is explained in Section 3.1. The sensor is moved from $c =$ P1 to $c =$ P2, then to $c =$ P3, and all other possible sensor locations from Fig. 3 while evaluating the measurement duration $T_h(c, 1)$ for all structural components h. All input parameters remain unchanged except the Fisher information changes, leading to a different maximum measurement duration for each sensor layout. For comparison, six sensor layouts are plotted in Fig. 6 together with the corresponding measurement duration (bright grey bars). The maximum measurement duration $T(c, 1) = \max_h\{T_h(c, 1)\}$ for each layout (grey bar) is copied into a performance chart and ranked, see Fig. 7. The optimum sensor layout is Configuration 8, as it exhibits the shortest measurement duration T_{opt} (dark grey bar). The sensor layouts with one sensor at position P3 or one sensor at P6 are not considered for damage diagnosis, because Mode 3 is unobservable at these locations, see Fig. 4. As a consequence, an unreasonably high measurement duration is obtained.

b) Genetic Algorithm

In the next study, tri-axial sensors are used at the possible sensor locations P1 - P8 instead of uni-axial sensors, so $r_{tot} = 24$ measurement channels are now available, see Fig. 3. Moreover, the number of channels is increased from one to $r = 3$ resulting in 2,024 different configurations according to Eq. (18). This is an appropriate case study to demonstrate the efficiency of the GA, as the number of sensor combinations is small enough for the ES method and large enough for the GA to become efficient.

First, the ES method is applied, and the layouts are ranked with respect to the measurement duration. The optimal performance is achieved if the vertical channels at the sensor locations P1, P4, and P8 are chosen, with the sensor layout plotted in Fig. 5 (right side). Secondly, the GA is launched while assigning the final rank (from the ES) to the elite members of each generation. For

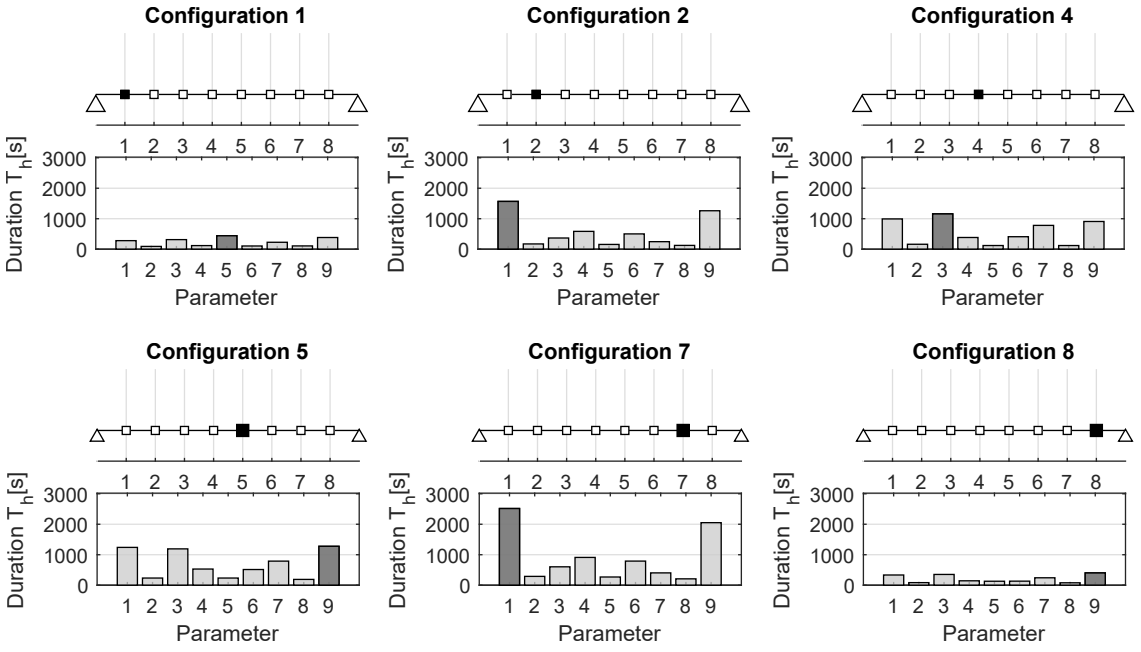

Figure 6: Calculating the measurement duration for all sensor configurations with one sensor, position P3 and P6 are not considered as Mode 3 is non-observable here

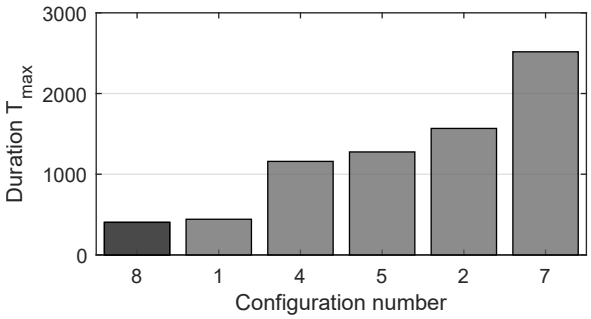

Figure 7: Ranking the configurations with respect to the maximum predicted measurement duration

example, if an elite member contains the optimum channel configuration from the ES, its rank is one, where the worst solution has a rank of 2,024.

The population size is set to 50 and the number of generations to 20. The elite count is set to 10%, meaning the best $0.1 \cdot 50 = 5$ sensor configurations survive to the next generation without modification. The cross-over fraction is set to 25%, so a quarter of all children, other than elite children, are made up of cross-over children. The results are summarized in a convergence chart, see Fig. 8. The GA effectively eliminates all layouts that exhibit sensors at the degrees of freedom in transverse and longitudinal direction, as expected, since only vertical modes of vibration are considered. It finds the global minimum within five generations, so $5 \cdot 50 = 250$ calculations of the objective function. That means the computation is sped up by a factor of $2,024/250 \approx 8$ in comparison to the ES. A close-to-optimal solution with a rank of 10 is already found within four generations and 200 calculation steps. In conclusion, the GA efficiently finds an appropriate sensor layout, and outperforms the ES even in this relatively small combinatorial problem.

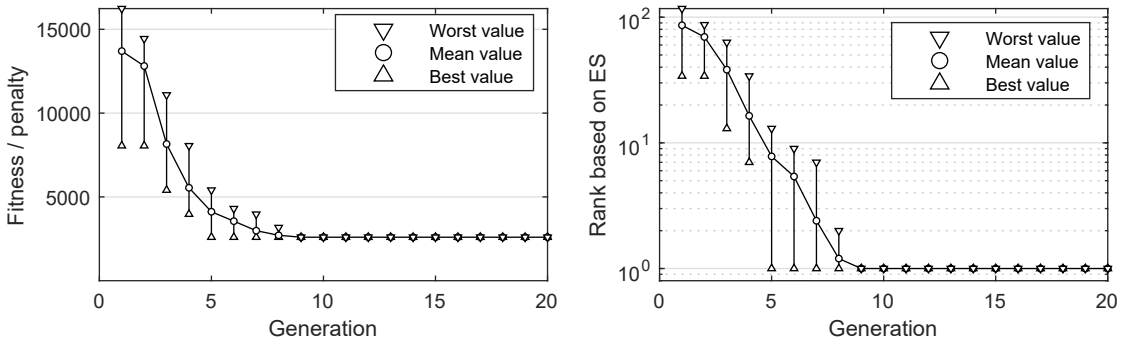

Figure 8: Convergence of the GA towards the optimal sensor layout, determined based on an ES

4.4. Appropriate Number of Sensors

The proposed sensor placement scheme can also be used to determine an acceptable number of sensors. In the preceding section, the optimization scheme was explained to find the optimal sensor configuration for a fixed number of sensors, where the optimal solution contains two pieces of information, i.e. the optimal sensor position and the corresponding measurement duration. The same procedure is now repeated for a varying number of sensors $r \in [1, \ldots, 4]$. For one to three sensors, the optimal sensor layout is plotted in Fig. 5. Plotting the optimal measurement duration T_{opt} over the corresponding number of sensors is a particularly intuitive way to understand the effect that an added sensor has on the performance of the damage detection method, see Fig. 9. With an increasing number of sensors, the slope gradually decreases, and at some point, adding additional sensors hardly improves the damage detectability. The elbow point, where the curve begins to flatten, can be an indicator for an appropriate number of sensors. Alternatively, the first best sensor configuration could be chosen as one that exhibits a measurement duration below the maximum allowable measurement duration T_{thres}, which was set to 240 s. In this case, two sensors seems to be an appropriate number of sensors.

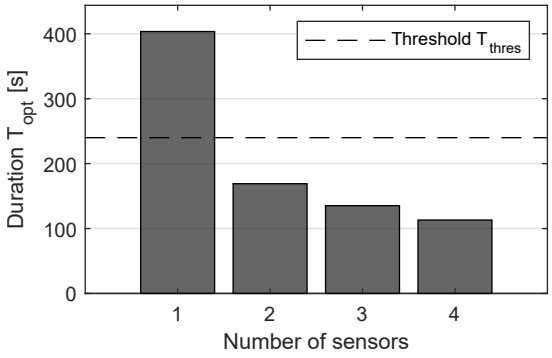

Figure 9: Increased test response due to an increasing number of sensors

5. Experimental Validation

Typically, the sensor placement optimization is performed before the structure is instrumented. Therefore, the optimization is performed based on simulated vibration data, as it is done in the

previous section. What remains to be shown is that the optimized sensor layout (based on simulated data) actually leads to higher damage detectability using real data.

The experimental validation is performed on a laboratory steel beam that was already described in Section 4.1. All signal processing parameters are identical and listed in Table B.1. The instrumentation consists of an electro-dynamic shaker (Mini Smartshaker, Model K2004E01) and eight tri-axial seismic sensors (Tromino Tromographs) at the sensor locations P1 - P8, see Fig. 3, synchronized through radio communication. In this study, only vertical vibration measurements are considered. Since damage was defined as a change in mass, non-destructive tests using extra masses can be used to simulate different damage scenarios. Two different damage scenarios are considered: and extra mass on beam component 5, as well as an extra mass on beam component 8, see Fig. 3.

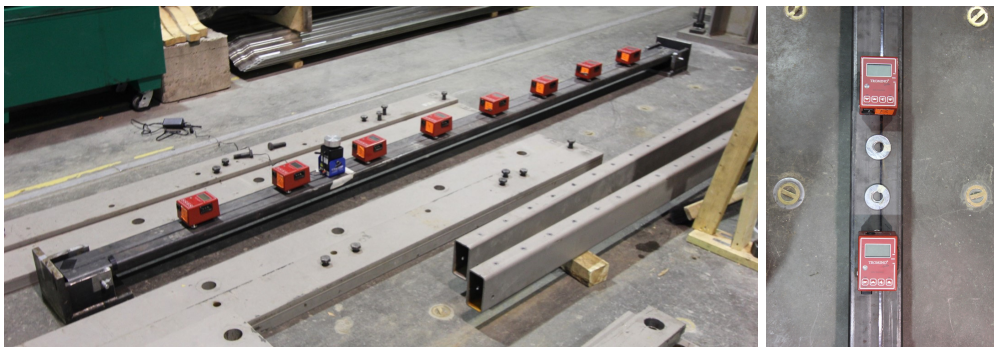

Figure 10: Photos of the laboratory experiment

In Section 4, the sensor layout was optimized for an optimal detectability across all beam components with $T(c,r) = \max\{T_1, \cdots, T_H\}$. However, this approach is not suitable for validation studies, because the masses are now only applied to component 5 or component 8, but the respective beam component might not lead to the decisive measurement duration. To remedy this, the performance criterion from Eq. (15) is modified to $T = T_5$ and $T = T_8$. In other words, the optimization procedure is rerun first to optimize the detectability in the beam components 5 and 8, respectively, and the damage detection results for the ranked sensor layouts are compared.

For validation, the damage detection test from Eq. (7) is applied to measured vibration data before and after an extra mass of 0.31 kg is applied, which corresponds to a relative change of mass by 5%. The test is applied 100 times so the empirical distribution can be plotted in histograms and the mean test response can be determined, as visualized in Fig. 11. Whereas the minimum measurement duration (from simulated data) is used as a performance criterion for optimal sensor placement, the mean test response (based on real data) is used as a validation criterion for the actual performance.

5.1. Optimized Sensor Layout

The primary purpose of the optimization scheme is to maximize damage detectability. Maximum detectability should lead to a minimum measurement duration during the sensor placement optimization, as well as a maximum mean test response during the laboratory test. If two sensors are to be placed at positions P1 - P8, $N_c = 28$ sensor combinations are possible.

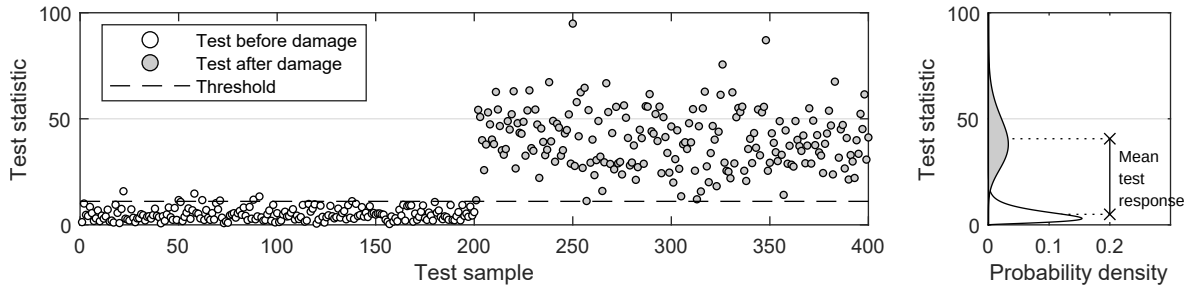

Figure 11: Validation scheme

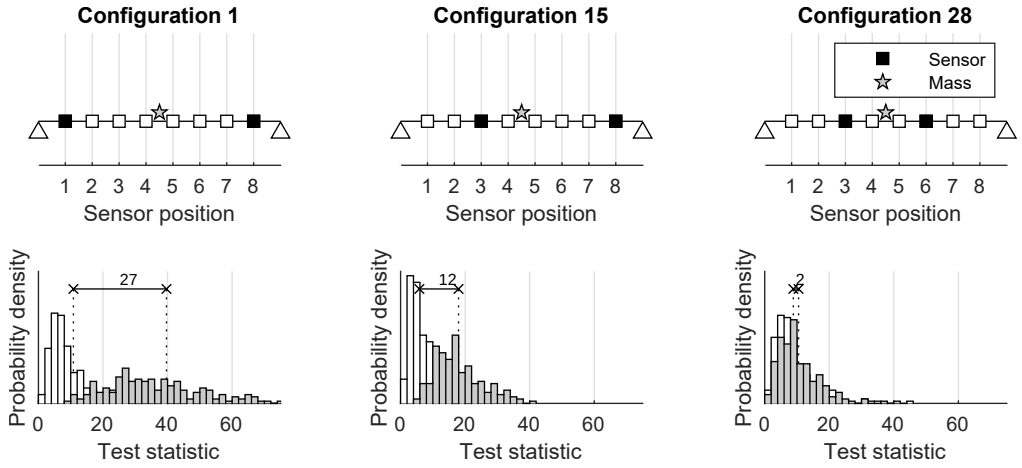

Figure 12: Optimizing the test sensor layout using T_5 (based on simulated data) and comparing the test response for real data with $\Delta_5 = 5\%$

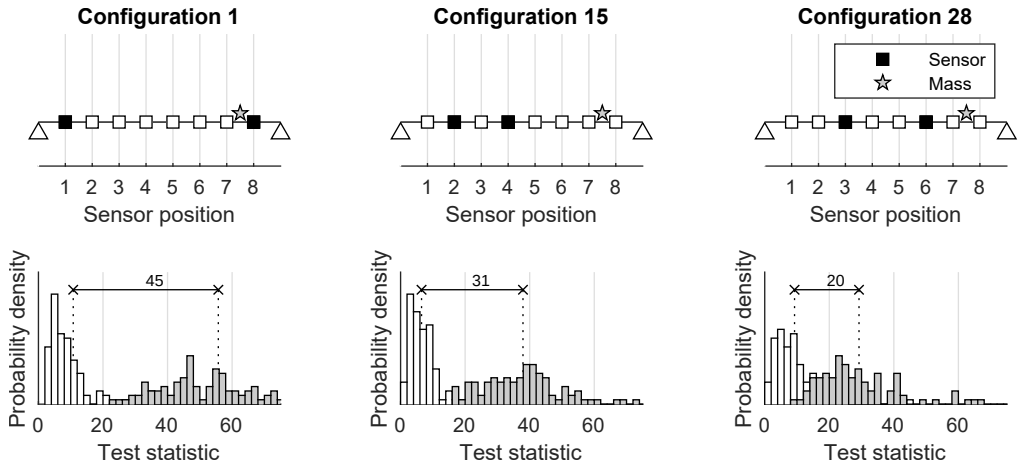

Figure 13: Optimizing the test sensor layout using T_8 (based on simulated data) and comparing the test response for real data with $\Delta_8 = 5\%$

Mass on component 5: First, the damage scenario with an extra mass at midspan is considered. Fig. 12 visualizes the sensor layout for the best sensor layout (left), the 15th best configuration (centre), and the worst sensor layout (right), together with the empirical mean test response that

was measured during the laboratory experiments. The respective mean test responses decrease from 45, to 31, and finally to 2. So, the worst configuration with sensors at P3 and P6 fails to detect the applied mass simply due to an inappropriate sensor placement. The result can be understood by looking at the mode shapes from Fig. 4. The sensor locations P3 and P6 are vibrational nodes of Mode 3, meaning no information from this mode of vibration is available for damage detection, resulting in a low Fisher information. In summary, a shorter measurement duration (based on simulated data) leads to a more pronounced mean test response for real data. This validates that the performance criterion is a measure for the detectability of damage and that the optimization can be performed based on simulated data.

Mass on component 8: Secondly, the scenario with a 5% extra mass near the supports is examined. Again, the best, the 15th best, and the worst sensor layouts are shown with corresponding mean test responses of 45, 31, and 20, so the sensor placement strategy successfully finds the optimal configuration. The reason why the sensor Configuration 15 in Fig. 13 is different than in Fig. 12 is because the measurement duration in individual components is used as a performance criteria instead of the maximum measurement duration over all components for validation ($T = T_8$ vs. $T = T_5$). It appears that the optimal sensor layout is the same for both damage scenarios (with sensors at P1 and P8), but an extra mass on Component 8 near the supports leads to a more pronounced response of the statistical test than with an extra mass on component 5 ($\lambda = 45$ vs. 27). This is consistent with the findings from Fig. 5 (middle), as the damage detectability (expressed through the required measurement duration) for component 8 is higher than for component 5 if the sensors are placed at positions P1 and P8.

5.2. Increased Number of Sensors

The results based on numerical simulations confirm the intuitive assumption that an increased number of sensors leads to higher damage detectability, so the measurement duration can also be used to decide on an appropriate number of sensors. To demonstrate this, the best configurations with one sensor, two sensors, and four sensors are illustrated in Fig. 14 together with the empirical distributions during the laboratory experiment. This figure clarifies that with an increasing number of sensors, the mean test response increases from over 30 to 41 and 46, which verifies that an increased number of sensors leads to higher damage detectability (Section 4.4 and Fig. 9).

6. Conclusion

This paper proposes a performance criterion for sensor placement optimization and explains how it can be combined with an adapted genetic algorithm (GA) to efficiently find a close-to-optimal solution for large structures. The primary purpose is to optimize the probability of detecting damages, where damage is defined as a deterioration of structural design parameters, such as material properties or cross-sectional values. Since damage detectability in all structural components with a limited number of sensors is unrealistic, the approach requires a prioritized set of damages scenarios whose detectability is optimized. Then, the approach is suitable to find an optimal sensor layout for a fixed number of sensors, as well as an appropriate number of sensors.

One aspect of the approach is that, although the damage diagnosis is based on global vibration measurements, it can be focused on the monitoring of local structural components that are critical for the safety or the serviceability of the structure. The proposed method requires the user to

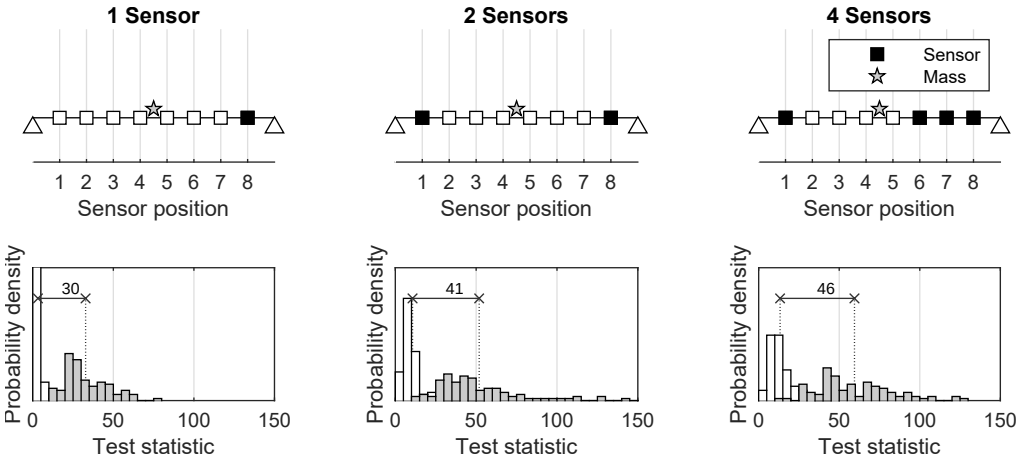

Figure 14: Increased test response due to an increasing number of sensors (only the optimal configurations are shown)

pre-select the structural parameters to be monitored and to define the detectable damage. This information tunes the sensor layout to become more sensitive to anticipated damage scenarios and yields a performance-based sensor layout. Another aspect is that the method considers the excitation and noise characteristics of the measured signals, captured through the covariance matrix of the damage-sensitive feature. Since real data is typically not available at all candidate positions, the covariance can be estimated based on simulated vibration data generated under realistic noise and excitation characteristics. Based on a laboratory steel beam, it is demonstrated that the findings based on simulated vibration records can be transferred to real structures, despite the noisy measurement environment and possibly different excitation levels. An interesting future study would be to take the leap from laboratory experiments to real-life structures; this will be the subject of future publications.

Acknowledgments

This work was supported by a strategic research grant from the Natural Sciences and Engineering Research Council of Canada, the German Academic Exchange Service, and a Mitacs Globalink Research Award.

Appendix A. Gaussian Residual Vectors

In this section, the stochastic subspace-based residual is recalled, as an exemplary residual vector that fulfills the CLT from Eq. (6). The residual vector is formed in the subspace of covariance functions (in the time domain), so it can be evaluated in quasi real-time. The output covariances $\mathbf{R}_i = E[\mathbf{y}_{k+i}\mathbf{y}_k^T]$ evaluate the similarities of output signals $\mathbf{y}$ (displacements, velocitities, or accelerations) at different sensor locations and time lags i [55]. When arranged in a block Hankel matrix $\boldsymbol{\mathcal{H}}$, with a size that is determined by the time lag parameters p and q, the dynamic properties of a vibrating structure can be retrieved from its column space. Using singular value decomposition,

the matrix can be decomposed into its singular values and vectors

$$\boldsymbol{\mathcal{H}} = \begin{bmatrix} \mathbf{R}_1 & \mathbf{R}_2 & \iddots & \mathbf{R}_q \\ \mathbf{R}_2 & \mathbf{R}_3 & \iddots & \mathbf{R}_{q+1} \\ \iddots & \iddots & \iddots & \iddots \\ \mathbf{R}_{p+1} & \mathbf{R}_{p+2} & \iddots & \mathbf{R}_{p+q} \end{bmatrix} = \begin{bmatrix} \mathbf{S}_1 & \mathbf{S}_0 \end{bmatrix} \begin{bmatrix} \mathbf{D}_1 & \mathbf{0} \\ \mathbf{0} & \mathbf{0} \end{bmatrix} \begin{bmatrix} \mathbf{W}_1^T \\ \mathbf{W}_0^T \end{bmatrix}. \tag{A.1}$$

The non-zero singular values in $\mathbf{D}_1$ are ranked in descending order and cut off after the system order $n = 2m$, where m is the number of modes that are present in the signal. Correspondingly, the left singular vectors are split into the column space $\mathbf{S}_1$ and the left null space $\mathbf{S}_0$. In the following, it is assumed that the matrix $\mathbf{S}_0$ is obtained in the reference state. Due to the orthogonality of the two vector spaces, it holds that $\mathbf{S}_0^T \boldsymbol{\mathcal{H}} = \mathbf{0}$ if and only if $\boldsymbol{\mathcal{H}}$ also corresponds to the reference state, since damage alters the dynamic properties in the block Hankel matrix. Hence, a damage-sensitive residual can be formed by pre-multiplying the left null space from reference data to the Hankel matrix estimate from incoming data

$$\boldsymbol{\varepsilon} = \mathrm{vec}\left(\mathbf{S}_0^T \hat{\boldsymbol{\mathcal{H}}}\right). \tag{A.2}$$

The hat symbol $\hat{(\cdot)}$ indicates that the block Hankel matrix is estimated based on a finite sample size N, using the sample covariance matrix $\hat{\mathbf{R}}_i = \frac{1}{N-i} \sum_{k=1}^{N-i} \mathbf{y}_{k+i} \mathbf{y}_k^T$. The vectorization operator $\mathrm{vec}(\cdot)$ stacks the columns of the residual matrix to obtain a residual vector that fulfills the CLT from Eq. (6).

Appendix B. Signal Processing Parameters

Data		**Segmenting**		**Processsing**	
Measured quantity	acceleration	Training segments	100	No. of sensors	varying
Sampling frequency	330 Hz	Testing segments	100	Time lags	$p + 1/q$=20
Reference data length	110 min	Samples/segment	9,900	System order	n=18
Training/testing data	110 min	Duration/segment	30 s	Block lengths	N_b=20

Table B.1: Input parameter sheet

References

[1] C. Farrar, K. Worden, Structural health monitoring: A machine learning perspective, Wiley, Oxford, U.K., 2012.

[2] T.-H. Yi, H.-N. Li, Methodology developments in sensor placement for health monitoring of civil infrastructures, International Journal of Distributed Sensor Networks 8 (8) (2012).

[3] W. Ostachowicz, R. Soman, P. Malinowski, Optimization of sensor placement for structural health monitoring: A review, Structural Health Monitoring 18 (3) (2019) 963–988.

[4] R. J. Barthorpe, K. Worden, Emerging trends in optimal structural health monitoring system design: From sensor placement to system evaluation, Journal of Sensor and Actuator Networks 9 (3) (2020) 31.

[5] J. P. de Clerck, P. Avitable, Development of several new tools for pre-test, in: Proceedings of SPIE 2768, 1996, pp. 1272–1277.

[6] Y. T. Chung, J. D. Moore, On-orbit sensor placement and system identification of space station with limited instrumentations, in: 11th International Modal Analysis Conference, Kissimmee, United States, February, 1993.
[7] C. B. Larson, D. C. Zimmermann, E. L. Marek, A comparison of modal test planning techniques: Excitation and sensor placement using the NASA 8 bay truss, in: 12th International Modal Analysis Conference, Honolulu, Hawaii, January, 1994, pp. 205–211.
[8] D. C. Kammer, Sensor placement for on-orbit modal identification and correlation of large space structures, Journal of Guidance, Control, and Dynamics 14 (2) (1991) 251–259.
[9] C. Boller, F.-K. Chang, Y. Fujino (Eds.), Encyclopedia of structural health monitoring, John Wiley & Sons, Chichester, United Kingdom, 2009.
[10] R. J. Allemang, D. L. Brown, A correlation coefficient for modal vector analysis, in: 1st International Modal Analysis Conference, Orlando, United States, May, 1982, pp. 110–116.
[11] R. N. Soman, T. Onoufriou, M. A. Kyriakides, R. A. Votsis, C. Z. Chrysostomou, Multi-type, multi-sensor placement optimization for structural health monitoring of long span bridges, Smart Structures and Systems 14 (1) (2014) 55–70.
[12] C. Papadimitriou, Optimal sensor placement methodology for parametric identification of structural systems, Journal of Sound and Vibration 278 (4-5) (2004) 923–947.
[13] K. V. Yuen, L. S. Katafygiotis, C. Papadimitriou, N. C. Mickleborough, Optimal sensor placement methodology for identification with unmeasured excitation, Journal of Dynamic Systems, Measurement, and Control 123 (4) (2001) 677–686.
[14] C. Papadimitriou, G. Lombaert, The effect of prediction error correlation on optimal sensor placement in structural dynamics, Mechanical Systems and Signal Processing 28 (2012) 105–127.
[15] S. Kumar, J. Seinfeld, Optimal location of measurements for distributed parameter estimation, IEEE Transactions on Automatic Control 23 (4) (1978) 690–698.
[16] V. Tzoumas, A. Jadbabaie, G. J. Pappas, Sensor placement for optimal kalman filtering: Fundamental limits, submodularity, and algorithms, in: American Control Conference, IEEE, Boston, MA, USA, 2016, pp. 191–196.
[17] M. Reynier, H. Abou-Kandil, Sensors location for updating problems, Mechanical Systems and Signal Processing 13 (2) (1999) 297–314.
[18] K. O. Kim, H. S. Yoo, Y. J. Choi, Optimal sensor placement for dynamic testing of large structures, in: 19th AIAA Applied Aerodynamics Conference, Anaheim, United States, 2001.
[19] C. Papadimitriou, Y. Haralampidis, K. Sobczyk, Optimal experimental design in stochastic structural dynamics, Probabilistic Engineering Mechanics 20 (1) (2005) 67–78.
[20] D. S. Li, H. N. Li, C. P. Fritzen, On optimal sensor placement criterion for structural health monitoring with representative least squares method, in: Key Engineering Materials, Vol. 413-414, Trans Tech Publications, Switzerland, June, 2009, pp. 383–391.
[21] Z. Shi, S. Law, L. Zhang, Optimum sensor placement for structural damage detection, Journal of Engineering Mechanics 126 (11) (2000) 1173–1179.
[22] J.-F. Lin, Y.-L. Xu, S. Zhan, Experimental investigation on multi-objective multi-type sensor optimal placement for structural damage detection, Structural Health Monitoring 18 (3) (2019) 882–901.
[23] R. F. Guratzsch, S. Mahadevan, Structural health monitoring sensor placement optimization under uncertainty, AIAA journal 48 (7) (2010) 1281–1289.
[24] D.-S. Li, Fritzen,, C.P, H.-N. Li, Extended minmac algorithm and comparison of sensor placement methods, in: 26th International Modal Analysis Conference, Orlando, United States, February, 2008.
[25] M. I. Friswell, R. Castro-Triguero, Clustering of sensor locations using the effective independence method, AIAA journal 53 (5) (2015) 1388–1391.
[26] J. H. Holland, Adaptation in natural and artificial systems, Ann Arbor: University of Michigan Press, Cambridge, United Kingdom, 1975.
[27] P. van Laarhoven, E. Aarts, Simulated annealing: Theory and applications, Springer Science & Business Media, Dordrecht, Netherlands, 1987.
[28] A. Corana, M. Marchesi, C. Martini, S. Ridella, Minimizing multimodal functions of continuous variables with the simulated annealing algorithm, ACM Transactions on Mathematical Software 13 (3) (1987) 262–280.
[29] R. Eberhart, J. Kennedy, A new optimizer using particle swarm theory, in: Sixth International Symposium on Micro Machine and Human Science, IEEE, Nagoya, Japan, 1995, pp. 39–43.
[30] T.-H. Yi, H.-N. Li, C.-W. Wang, Multiaxial sensor placement optimization in structural health monitoring using distributed wolf algorithm, Structural Control and Health Monitoring 23 (4) (2016) 719–734.
[31] G. Overton, K. Worden, Sensor optimisation using an ant colony metaphor, Strain 40 (2) (2004) 59–65.
[32] M. Scott, K. Worden, A bee swarm algorithm for optimising sensor distributions for impact detection on a

composite panel, Strain 51 (2) (2015) 147–155.
[33] G. D. Zhou, T. H. Yi, H. N. Li, Sensor placement optimization in structural health monitoring using cluster-in-cluster firefly algorithm, Advances in Structural Engineering 17 (8) (2014) 1103–1115.
[34] S. Feng, J. Jia, Acceleration sensor placement technique for vibration test in structural health monitoring using microhabitat frog-leaping algorithm, Structural Health Monitoring 17 (2) (2018) 169–184.
[35] T.-H. Yi, H.-N. Li, X.-D. Zhang, Health monitoring sensor placement optimization for canton tower using immune monkey algorithm, Structural Control and Health Monitoring 22 (1) (2015) 123–138.
[36] M. Basseville, L. Mevel, M. Goursat, Statistical model-based damage detection and localization: subspace-based residuals and damage-to-noise sensitivity ratios, Journal of Sound and Vibration 275 (3-5) (2004) 769–794.
[37] M. Döhler, L. Mevel, F. Hille, Subspace-based damage detection under changes in the ambient excitation statistics, Mechanical Systems and Signal Processing 45 (1) (2014) 207–224.
[38] M. Döhler, L. Mevel, Q. Zhang, Fault detection, isolation and quantification from Gaussian residuals with application to structural damage diagnosis, Annual Reviews in Control 42 (2016) 244–256.
[39] A. Mendler, M. Döhler, C. E. Ventura, A reliability-based approach to determine the minimum detectable damage for statistical damage detection, Mechanical Systems and Signal Processing 154 (2021) 107561.
[40] A. Mendler, Minimum diagnosable damage and optimal sensor placement for structural health monitoring, Ph.D. thesis, University of British Columbia, Vancouver, Canada (2020).
[41] M. Basseville, M. Abdelghani, A. Benveniste, Subspace-based fault detection algorithms for vibration monitoring, Automatica 36 (1) (2000) 101–109.
[42] P. Mellinger, M. Döhler, L. Mevel, Variance estimation of modal parameters from output-only and input/output subspace-based system identification, Journal of Sound and Vibration 379 (2016) 1–27.
[43] G. Oliveira, F. Magalhães, Á. Cunha, E. Caetano, Vibration-based damage detection in a wind turbine using 1 year of data, Structural Control and Health Monitoring 25 (11) (2018) e2238.
[44] S. Greś, M. Döhler, P. Andersen, L. Mevel, Subspace-based Mahalanobis damage detection robust to changes in excitation covariance, Structural Control and Health Monitoring (2021) e2760.
[45] E. Viefhues, M. Döhler, F. Hille, L. Mevel, Statistical subspace-based damage detection with estimated reference, Mechanical Systems and Signal Processing 164 (2022) 108241.
[46] E. Balmès, M. Basseville, F. Bourquin, L. Mevel, H. Nasser, F. Treyssède, Merging sensor data from multiple temperature scenarios for vibration monitoring of civil structures, Structural Health Monitoring 7 (2) (2008) 129–142.
[47] E. Viefhues, M. Döhler, F. Hille, L. Mevel, Fault detection for linear parameter varying systems under changes in the process noise covariance, in: 21st IFAC World Congress, Berlin, Germany, 2020.
[48] F. Magalhães, Á. Cunha, E. Caetano, Vibration based structural health monitoring of an arch bridge: from automated OMA to damage detection, Mechanical Systems and Signal Processing 28 (2012) 212–228.
[49] A. Benveniste, M. Basseville, G. Moustakides, The asymptotic local approach to change detection and model validation, IEEE Transactions on Automatic Control 32 (7) (1987) 583–592.
[50] S. Allahdadian, M. Döhler, C. Ventura, L. Mevel, Towards robust statistical damage localization via model-based sensitivity clustering, Mechanical Systems and Signal Processing 134 (2019) 106341.
[51] M. Basseville, A. Benveniste, G. Moustakides, A. Rougée, Optimal sensor location for detecting changes in dynamical behavior, IEEE Transactions on Automatic Control 32 (12) (1987) 1067–1075.
[52] K. Deb, Multi-objective optimization using evolutionary algorithms, John Wiley & Sons, Ltd, Chichester, United Kingdom, 2001.
[53] A. Messac, Optimization in practice with MATLAB: For engineering students and professionals, Cambridge University Press, New York, United States, 2015.
[54] J. Yang, C. K. Soh, Structural optimization by genetic algorithms with tournament selection, Journal of Computing in Civil Engineering 11 (3) (1997) 195–200.
[55] R. Brincker, C. E. Ventura, Introduction to operational modal analysis, John Wiley & Sons, Chichester, United Kingdom, 2015.